Increased Energy Expenditure and Protection From Diet-Induced Obesity in Mice Lacking the cGMP-Specific Phosphodiesterase PDE9

Ryan P. Ceddia,[1,2] Dianxin Liu,[1,2] Fubiao Shi,[1,2] Mark K. Crowder,[3] Sumita Mishra,[4] David A. Kass,[4,5,6] and Sheila Collins[1,2,7]

Cyclic nucleotides cAMP and cGMP are important second messengers for the regulation of adaptive thermogenesis. Their levels are controlled not only by their synthesis, but also their degradation. Since pharmacological inhibitors of cGMP-specific phosphodiesterase 9 (PDE9) can increase cGMP-dependent protein kinase signaling and uncoupling protein 1 expression in adipocytes, we sought to elucidate the role of PDE9 on energy balance and glucose homeostasis in vivo. Mice with targeted disruption of the PDE9 gene, *Pde9a*, were fed nutrient-matched high-fat (HFD) or low-fat diets. *Pde9a*$^{-/-}$ mice were resistant to HFD-induced obesity, exhibiting a global increase in energy expenditure, while brown adipose tissue (AT) had increased respiratory capacity and elevated expression of *Ucp1* and other thermogenic genes. Reduced adiposity of HFD-fed *Pde9a*$^{-/-}$ mice was associated with improvements in glucose handling and hepatic steatosis. Cold exposure or treatment with β-adrenergic receptor agonists markedly decreased *Pde9a* expression in brown AT and cultured brown adipocytes, while *Pde9a*$^{-/-}$ mice exhibited a greater increase in AT browning, together suggesting that the PDE9-cGMP pathway augments classical cold-induced β-adrenergic/cAMP AT browning and energy expenditure. These findings suggest PDE9 is a previously unrecognized regulator of energy metabolism and that its inhibition may be a valuable avenue to explore for combating metabolic disease.

The lack of effective therapies for the obesity epidemic is a serious challenge, as recent studies report that ∼40% of Americans are clinically obese, with the prevalence of obesity rising worldwide (1). Obesity is comorbid with insulin resistance and type 2 diabetes along with other chronic illnesses, such as cardiovascular diseases, nonalcoholic fatty liver disease, asthma, and certain cancers (2). Thus, finding ways to treat or reduce obesity are important for decreasing diabetes and related diseases. At its simplest, obesity can be managed by either reducing the calories consumed or by increasing energy expenditure. Changes in diet and exercise are the most commonly recommended methods to treat obesity, but rarely succeed over the long-term (3). Much effort has been directed toward reducing caloric intake, including pharmacological approaches such as appetite suppressants and blockade of fat absorption (4). These are frequently accompanied by unacceptable side effects or eventual lack of efficacy. Invasive procedures such as bariatric surgery have also been prescribed (4), and while to date, this approach has proven effective at ameliorating insulin resistance and providing sustained weight loss, the risks associated with such radical surgeries should not be underestimated (5). Alternatively, one potential means to increase energy expenditure aside from physical exercise is energy-consuming futile metabolic cycles and uncoupled respiration (6).

Brown adipose tissue (BAT) in mammals is a mechanism for maintaining body temperature. Brown adipocytes can regulate uncoupled respiration via oxidative metabolism that generates heat without ATP synthesis. These adipocytes contain a unique mitochondrial protein called uncoupling protein 1 (UCP1). When activated, UCP1 is a gated pore that allows H^+ to pass through the inner mitochondrial membrane, thereby uncoupling oxidative phosphorylation from ATP production (7). While UCP1 is the signature protein of BAT, it can also be expressed in cells of white adipose tissue (WAT) in response to stimuli that increase cyclic nucleotides (i.e., cAMP and cGMP). These WAT adipocytes that have a brownlike phenotype are sometimes called "beige" adipocytes (8,9). During the last decade, there has been growing appreciation that adult humans possess significant amounts of brown and beige adipocytes that are rich in mitochondria and UCP1 (10–13). Thus, activation of brown/beige adipocyte thermogenesis to increase net energy expenditure might be an attractive therapeutic target for obesity and metabolic disease.

Increasing the concentration of cyclic nucleotides cAMP and cGMP in adipocytes is associated with an increase in UCP1 expression and thermogenic activity (14–17). For cAMP, this is classically observed in response to cold temperature, leading to increased secretion of norepinephrine from sympathetic nerves that activate the adipocyte's β-adrenergic receptors (AR) (18). In addition to the important physiological role of the sympathetic nervous system and catecholamines, we and other have shown that the cardiac natriuretic peptides (NP), atrial NP (ANP) and B-type NP (BNP), are also capable of increasing thermogenic activity of adipocytes via increasing intracellular cGMP and thereby exert antiobesity effects (19–25). Levels of cyclic nucleotides are controlled not only by their synthesis, but also their degradation. The phosphodiesterase (PDE) enzymes break the phosphodiester bond in cyclic nucleotides, rendering them inactive (26). Based on our new findings that cold exposure decreases the expression of cGMP-specific PDE9, one of the most selective PDEs to degrade cGMP over cAMP (27), we asked whether decreasing the degradation of cGMP would have similar prothermogenic and antiobesity effects. The safe clinical utility for pharmacological inhibition of several PDEs has been demonstrated for a number of diseases, and the inhibition of multiple PDEs has been associated with increased adipocyte browning (reviewed in Ref. 17). Several small-molecule PDE9 inhibitors have entered clinical trials for conditions such as Alzheimer disease, schizophrenia, and sickle cell disease in which their safety has been established (28–34).

We hypothesized that the absence of PDE9 would counteract diet-induced weight gain and improve glucose handling via increasing uncoupled energy expenditure. We used a global *Pde9a* knockout mouse and show that these *Pde9a*$^{-/-}$ mice resist diet-induced weight gain and have concomitant improvements associated with reduced adiposity. Changes in energy expenditure associated with *Pde9a* knockout at any given time were small; however, over the extended course of the study, these modest changes became significant, leading to a reduced body weight and adiposity. As most people become obese slowly, gaining ~0.5–1.0 kg/year (35,36), we posit that inhibition of PDE9 may be useful for counteracting this slow weight gain over time.

RESEARCH DESIGN AND METHODS

Materials
See Supplementary Table 1 for more information.

Animals
Animal studies were conducted at Sanford Burnham Prebys Medical Discovery Institute (SBP), Vanderbilt University Medical Center (VUMC), and Johns Hopkins University and School of Medicine (JHSOM). *Pde9a*$^{-/-}$ mice on a C57BL/6J background were previously described (37). Mice were maintained on a 12-h light/dark cycle with two to five animals per cage and ad libitum food and water. At 6 weeks of age, SBP and VUMC mice received nutrient-matched Surwit diets: a control low-fat diet (LFD) (10.5% calories from fat: D12328; Research Diets) or high-fat diet (HFD) (58.0% calories from fat: D12330; Research Diets). JHSOM mice were fed HFD (60.0% calories from fat: D12492; Research Diets). Mice were weighed twice weekly, and body composition was measured using a Minispec Body Composition Analyzer (Bruker) at SBP and Vanderbilt Mouse Metabolic Phenotyping Center (VMMPC) or EchoMRI-100 (Echo Medical Systems) at JHSOM. Mice were fasted for 5-h prior to euthanasia by CO_2 asphyxiation and exsanguination via cardiac puncture. All procedures were approved by the Institutional Animal Care and Use Committees at SBP, VUMC, and JHSOM.

Cold Exposure and β₃-AR Agonist
Chow-fed 13–16-week-old male mice were housed at 30°C for 2–4 days prior to habitation at 6°C for the indicated times. Additional mice received intraperitoneal CL-316,243 (1 mg/kg body weight/day) for 1 week as in Liu et al. (38).

Cell Culture
IngJ6 and Bat8 immortalized mouse cell lines (8) and human multipotent adipose-derived stem cells (hMADS) (39) were cultured and differentiated as described.

Quantitative Real-time RT-PCR
RNA was extracted using TRIzol and the aqueous phase purified on Zymo-Spin IIICG Columns. Instruments used were the Roche LightCycler 480 II or Applied Biosystems QuantStudio 6 Flex System. Three replicates of each sample were averaged, normalized to *mRplp0* (36B4), and analyzed using the Pfaffl method. Primer sequences are in Supplementary Table 2.

Western Blotting

Western blotting was as described (24). Image acquisition was on Bio-Rad Digital ChemiDoc MP with IR or Typhoon FLA9000 Variable Mode Imager.

Histology

Tissues were fixed in 10% formaldehyde (4°C overnight) and stored in 70% ethanol (4°C). Histology was performed by the Vanderbilt Translational Pathology Shared Resource. Slides were imaged at ×20 original magnification with a Leica SCN400 Slide Scanner in the Digital Histology Shared Resource.

Triglyceride Composition

Lipids were extracted from frozen liver and quantified by the VMMPC Lipid Core.

Glucose and Insulin Sensitivity

For both the glucose tolerance test (GTT) and insulin tolerance test (ITT), mice were fasted for 5-h during the light cycle. Intraperitoneal injections of 1.0 g/kg dextrose in 0.9% saline for GTT or 0.5 units/kg insulin in 0.9% saline for ITT. Glucose was measured from tail-vein blood with a Bayer CONTOUR glucometer and glucose test strips. Clamp studies were done in chronically catheterized conscious mice by the VMMPC.

Fasting Blood Glucose, Plasma Insulin, and Plasma Chemistry

Prior to euthanasia, mice were fasted for 5 h, and glucose was measured from tail-vein blood. Mice were euthanized, and plasma was obtained from blood via cardiac puncture into tubes containing 8 μL of 0.5 mol/L EDTA. Insulin was measured from plasma stored at −80°C by ELISA. ALT, triglyceride, and cholesterol quantification was performed on plasma stored at −20°C by the Vanderbilt Translational Pathology Shared Resource.

Energy Balance

Mice used for energy balance studies were maintained at VUMC and JHSOM and fed HFD for 15 and 26 weeks, respectively. Indirect calorimetry and measurements of food intake and physical activity were performed on mice in the Promethion System (Sable Systems International) by the VMMPC or the Comprehensive Lab Animal Monitoring System (CLAMS) by the Rodent Metabolism Core at JHSOM. Light and dark cycles were analyzed independently.

BAT Respirometry

High-resolution respirometry was performed using Oxygraph-2k (Oroboros Instruments) in the VMMPC. Interscapular BAT (iBAT) from age-matched chow-fed mice was dissected into 1.6–2.5-mg pieces and permeabilized by sequential incubation in biopsy preservation solution (BIOPS), BIOPS plus saponin, and MiR05, each for 20 min at 4°C. Assays were performed in MiR05 at 37°C,

and substrates were added in the order indicated. Data were normalized to wet tissue weight.

Statistics

Data are mean ± SEM using Prism version 9.1.0 for Windows 64-bit (GraphPad Software). Unless otherwise stated, analyses were performed using two-way ANOVA. Post hoc analyses of ANOVA used Sidak multiple comparisons test for *Pde9a* genotype only and indicated on figures with the symbols: *$Pde9a^{+/+}$ versus $Pde9a^{-/-}$, †$Pde9a^{+/+}$ versus $Pde9a^{+/-}$, and ‡$Pde9a^{+/-}$ versus $Pde9a^{-/-}$; and one symbol, $P < 0.05$; two symbols, $P < 0.01$; or three symbols, $P < 0.001$. For analyses of body mass and blood glucose over time, two-way ANOVA with repeated measures was performed comparing the factors *Pde9a* genotype and time, analyzing diet groups independently. Average energy expenditure, VO_2, and respiratory quotient for light and dark cycles were analyzed using the least squares method of multiple linear regression with model including the continuous effect of body mass and the categorical effects of diet, genotype, and instrument (i.e., Promethion at VUMC or CLAMS at JHSOM).

Data and Resource Availability

Data/resources are available upon request from the corresponding author.

RESULTS

Loss of PDE9 Facilitates Cold-Mediated AT Browning

We and others previously established that the cGMP–cGMP-dependent protein kinase (PKG) signaling axis in adipocytes can increase brown and beige adipocyte activity, including mitochondrial biogenesis, UCP1 expression, uncoupled respiration, and energy expenditure (19–25,40–42). In addition, the dynamic control of the ratio between the guanylyl cyclase-containing NP receptor, NPRA, to the clearance receptor, NPRC, is an important regulator of NP signaling (reviewed in Ref. 17), and we previously showed that cold temperature exposure reduces expression of NPRC (20). Given that PDE5 and PDE9 are selective for degrading cGMP, we sought to determine if they also played a role in the brown fat thermogenic program. *Pde5a* and *Pde9a* expression were measured in iBAT following both short-term and long-term cold exposure. We found that *Pde9a*, but not *Pde5a*, gene expression was significantly suppressed by cold exposure at both time points (Fig. 1A–D). A similar suppression of *Pde9a*, but not *Pde5a*, expression in iBAT was found in mice treated with the β₃-AR agonist CL-316,243 (Fig. 1E and F). In an immortalized brown adipocyte cell line (Bat8), *Pde9a* expression was reduced in response to the β-AR agonist isoproterenol in a comparable manner (Fig. 1G and H). These findings indicate that cold-induced β-AR signaling suppresses *Pde9a*, but not *Pde5a*, gene expression.

As these findings suggest that a reduction in *Pde9a* may be important for cold-mediated induction of the brown fat thermogenic program, we asked whether global loss of
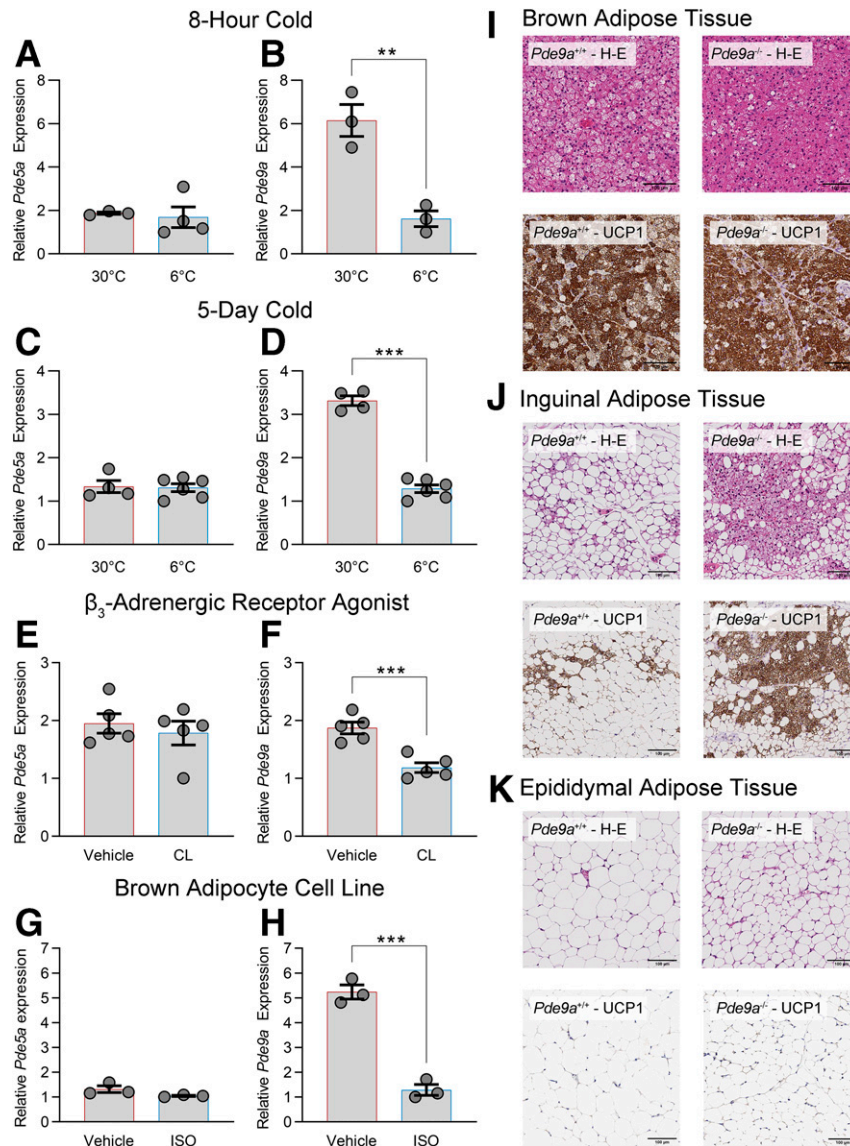
Figure 1—Cold exposure and β_3-adrenergic signaling suppresses *Pde9a* gene expression, while loss of PDE9 amplifies the cold-induced thermogenic program. Chow-fed male mice were exposed to cold for 8 h, and expression of *Pde5a* (*A*) and *Pde9a* (*B*) was measured in iBAT. $N = 3$ 30°C and $N = 3–4$ 6°C mice. Chow-fed male mice were exposed to cold for 5 days, and iBAT expression of *Pde5a* (*C*) and *Pde9a* (*D*) was measured. $N = 4$ 30°C and $N = 6$ 6°C mice. Chow-fed male mice were treated with vehicle or β_3-AR agonist CL-316,243 (CL) for 1 week, and expression of *Pde5a* (*E*) and *Pde9a* (*F*) in iBAT was measured. $N = 5$ vehicle and $N = 5$ CL mice. *Pde5a* (*G*) and *Pde9a* (*H*) in Bat8 adipocytes. Cells were serum starved for 2 h prior to treatment with vehicle or 10 μmol/L isoproterenol (ISO) for an additional 4 h. Three independent experiments are shown. All data are mean ± SEM, and analyses were performed using unpaired *t* test. Histology of iBAT (*I*), iWAT (*J*), and eWAT (*K*) from chow-fed male mice housed at 6°C for 3 days. Representative H-E– and UCP1-stained sections from $N = 3$ $Pde9a^{+/+}$ and $N = 3$ $Pde9a^{-/-}$ mice. **$P < 0.01$, ***$P < 0.001$.

PDE9 would affect AT browning. Male $Pde9a^{+/+}$ and $Pde9a^{-/-}$ mice were exposed to cold temperature for 3 days to cause a mild induction of the thermogenic program. $Pde9a^{-/-}$ mice demonstrated a significant increase in the amount of UCP1$^+$ adipocytes in their inguinal WAT (iWAT), while both iBAT and epididymal WAT (eWAT) appeared to have a reduction in adipocyte size (Fig. 1*I–K*). Together, these findings suggest that PDE9 is a negative regulator of the cold-mediated BAT thermogenic program.

PDE9 Inhibition Increases ANP-Evoked PKG Signaling and UCP1 Expression

We asked whether blocking PDE9 activity in adipocytes in vitro using small-molecule inhibitors would increase PKG signaling and the adipocyte thermogenic program. We used mouse cell lines representative of white (IngJ6) and brown (Bat8) adipocytes (8), hMADS (43), and two different PDE9 inhibitors: BAY73–6691 (BAY) and PF-04447943 (PF). As shown in Fig. 2*A* and *B*, phosphorylation of vasodilator-stimulated phosphoprotein (VASP) at

serine 239, a marker of PKG signaling (44), was increased in both IngJ6 and Bat8 cells treated with BAY above the level seen with ANP alone. BAY also slightly increased VASP phosphorylation in IngJ6 independent of ANP (Fig. 2A). The PF compound was also tested in Bat8 cells, where it increased ANP-evoked VASP[(S239)] phosphorylation in a dose-dependent manner (Fig. 2C). The hMADS cell line can express thermogenic markers and increase mitochondrial biogenesis after differentiation in response to catecholamines as well as cardiac NPs (20,39,43). We stimulated cGMP-PKG signaling by including the NPs, ANP and BNP, and/or PF during the last 7 days of differentiation. As shown in Fig. 2D, both the NPs and PF were able to increase UCP1 expression. Also shown is that the cell-permeable cGMP analog pCPT-cGMP raised UCP1 expression (Fig. 2D).

Protection From HFD-Induced Obesity by *Pde9a* Knockout

To test our hypothesis that PDE9 ablation would improve diet-induced obesity and glucose handling, male $Pde9a^{+/+}$, $Pde9a^{+/-}$, and $Pde9a^{-/-}$ mice were fed nutrient-matched control LFD or HFD for 16 weeks beginning at 6 weeks of age. Overall, *Pde9a* genotype affected body weight and body weight gain throughout the feeding study (Fig. 3A–D and Supplementary Fig. 1). The reduced body weight of HFD-fed $Pde9a^{-/-}$ was attributed to a reduction in fat mass (Fig. 3E

and *G*). Of note, $Pde9a^{+/-}$ mice exhibited an intermediate obesity phenotype when challenged with HFD. These data demonstrate that even haploinsufficiency of *Pde9a* confers resistance to HFD. Female $Pde9a^{-/-}$ mice also gained less weight than $Pde9a^{+/+}$ throughout the 16 weeks of HFD feeding (Supplementary Fig. 2). Compared with males, the differences in body weight were not as pronounced, but were also a result of reduced fat mass.

Improvements in Glucose Handling Are Proportional to Reduced Body Weight of $Pde9a^{-/-}$ Mice

Intraperitoneal GTT (IP-GTT) and IP-ITT were used to assess glucose handling and insulin sensitivity in male mice. In mice fed LFD, *Pde9a* genotype did not affect glucose handling. For HFD-fed mice, glucose tolerance was essentially identical between $Pde9a^{+/+}$ and $Pde9a^{+/-}$ mice, while $Pde9a^{-/-}$ mice exhibited a modest improvement (Fig. 4A and B and Supplementary Fig. 3A). ITT revealed very little difference between the *Pde9a* genotypes (Fig. 4C and Supplementary Fig. 3B and C). Fasting glucose and insulin levels were not significantly different (Fig. 4D and E). These findings are consistent with other observations in this study that modest increases in "adipose browning" and energy expenditure are sufficient to mitigate the more overt features of insulin resistance. In female mice on HFD, absence of *Pde9a* was also associated with a modest improvement in IP-GTT and IP-ITT
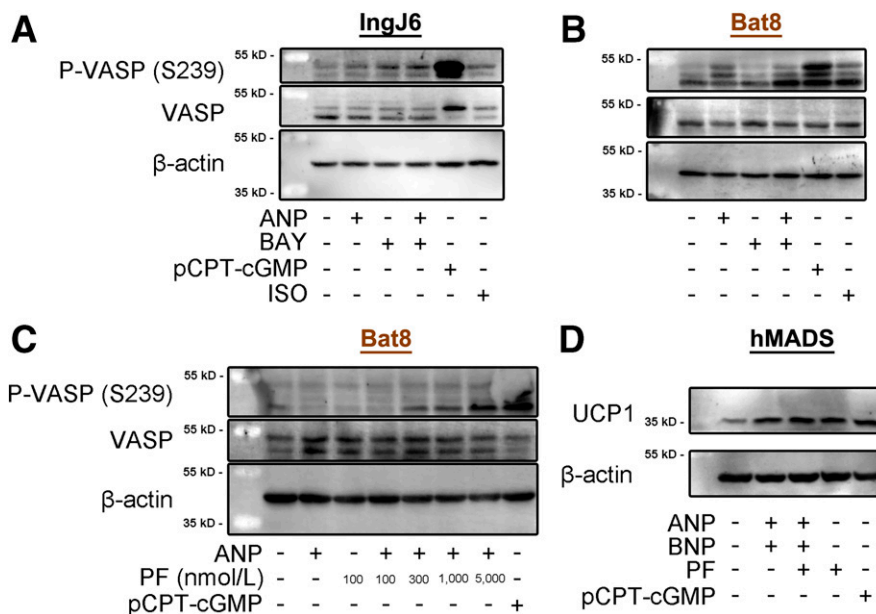

Figure 2—PDE9 inhibitors increase PKG signaling and UCP1 expression in adipocytes. IngJ6 (*A*) and Bat8 (*B*) adipocytes were serum starved overnight and treated with 5 μmol/L BAY for 90 min and 100 nmol/L ANP, 500 μmol/L pCPT-cGMP, or 1 μmol/L isoproterenol (ISO) for 60 min. Phosphorylation of VASP at Ser[239] is an indicator of PKG activity, as this is the major PKG phosphorylation site. The shift from 46 kDa to 50 kDa is due to phosphorylation at Ser[157], which can be phosphorylated by both cAMP-dependent protein kinase and PKG (44). Blots are representative of three similar experiments. *C*: Bat8 adipocytes were serum starved overnight and then treated with increasing concentrations of PF for 60 min and 100 nmol/L ANP or 500 μmol/L pCPT-cGMP for 30 min. Blots are representative of two similar experiments. *D*: hMADS were differentiated for 9 days, after which 200 nmol/L ANP, 200 nmol/L BNP, 300 nmol/L PF, and 200 μmol/L pCPT-cGMP were added for the remaining 7 days of differentiation. Blots are representative of three similar experiments.

(Supplementary Fig. 4A–F). Fasting glucose and insulin levels were not different (Supplementary Fig. 4G and H). Hyperinsulinemic-euglycemic clamps were performed in chronically catheterized conscious mice from another cohort of $Pde9a^{+/+}$ and $Pde9a^{-/-}$ male mice that were fed HFD for 16 weeks. The body weights of these mice were closely matched, thus controlling for the previous weight difference. In these mice, all measurements were largely the same between the $Pde9a^{+/+}$ and $Pde9a^{-/-}$ mice (Supplementary Fig. 3D–F). $Pde9a^{-/-}$ mice showed an increase in fasting glucose turnover rate; however, the rates of glucose uptake and endogenous glucose production during the hyperinsulinemic clamp were similar (Supplementary Fig. 3G).

To assess insulin signaling in AT, phosphorylation of AKT at Ser^{473} was measured postmortem in eWAT, iWAT, and iBAT (Fig. 4F). Three representative mice were chosen from each genotype × diet treatment group based upon their closeness to the mean terminal body weight of their group. Loss of $Pde9a$ was associated with increased AKT phosphorylation and therefore insulin signaling in AT regardless of dietary treatment (Fig. 4F).

Protection From HFD-Induced AT Expansion and Liver Damage in $Pde9a^{-/-}$ Mice

The reduction in body weight and adiposity in $Pde9a^{-/-}$ male mice was associated with reduced liver mass. Consistent with the observation that overall fat mass was lower in $Pde9a^{-/-}$ mice on HFD, the weights of individual adipose depots that were collected exhibited a similar trend (Fig. 5A–C). This also corresponded to a reduction in adipocyte size (Fig. 5D–F). On HFD, the iBAT of $Pde9a^{+/+}$ mice had large unilocular adipocytes, whereas $Pde9a^{-/-}$ had smaller multilocular adipocytes (Fig. 5F). In female mice on HFD, tissue weights exhibited a similar trend toward reduced mass in the $Pde9a^{-/-}$, which was particularly evident for iWAT and iBAT (Supplementary Fig. 5). In the liver, absence of $Pde9a$ led to a greater protection during HFD feeding. Hematoxylin and eosin (H-E) staining of the livers revealed prominent steatosis in the $Pde9a^{+/+}$ HFD-fed mice, which was significantly reduced in the HFD fed $Pde9a^{-/-}$ livers (Fig. 5G). This corresponded to a significant reduction in liver weight in $Pde9a^{-/-}$ mice (Fig. 5H). Once again, $Pde9a^{+/-}$ mice showed an intermediate reduction in liver weight. As expected, we observed a strong trend toward reduced hepatic triglyceride levels in the HFD-fed $Pde9a^{-/-}$ mice (Fig. 5I), with minor differences in fatty acid composition between genotypes (Supplementary Table 3). Hepatic steatosis frequently leads to liver damage. Circulating levels of plasma ALT, a biomarker of hepatocyte membrane damage, were measured. In the $Pde9a^{-/-}$ mice, ALT levels were significantly reduced (Fig. 5J). Plasma triglyceride levels were unchanged and cholesterol showed a trend toward being reduced in HFD-fed $Pde9a^{-/-}$ mice (Supplementary Fig. 6). Absence of $Pde9a$ was also associated with a significant reduction in heart and spleen weight and a trend toward reduced kidney weight with HFD feeding (Fig. 5K–L).

Increased Energy Expenditure in $Pde9a^{-/-}$ Mice

To determine whether there were differences in energy expenditure that would account for the differences in body weights and fat mass in HFD-fed $Pde9a^{-/-}$ mice, indirect calorimetry was measured on male mice at the end of the diet period. As shown in Supplementary Fig. 7, food intake and physical activity cannot account for the decreased weight and fat mass in the $Pde9a^{-/-}$ mice. Importantly, we found significantly increased energy expenditure ($P = 0.047$) and a trend toward increased oxygen consumption ($P = 0.057$) in $Pde9a^{-/-}$ mice during the dark cycle (Fig. 6A and B). Respiratory quotient was not changed (Fig. 6C).

Increased Thermogenesis-Related Gene Expression in the AT of $Pde9a^{-/-}$ Mice

We hypothesized that the increased energy expenditure in $Pde9a^{-/-}$ mice was due to increased PKG signaling and thermogenesis in the AT. Significant changes in resting VASP$^{(S239)}$ phosphorylation were not observed in iBAT or iWAT (Supplementary Fig. 8). It is likely that differences in unstimulated VASP$^{(S239)}$ phosphorylation are difficult to observe in vivo due to the continuous interplay of basal stimuli and dephosphorylation events. However, as shown in Fig. 7, a signature group of genes involved in energy expenditure was increased in the ATs of male $Pde9a^{-/-}$ mice. Compared with $Pde9a^{+/+}$ mice, in $Pde9a^{-/-}$ mice fed LFD, these genes were increased in iWAT, while in HFD-fed mice, these genes were increased in iBAT. Once again, in the $Pde9a^{+/-}$ mice, expression of each of these genes was intermediate between the $Pde9a^{+/+}$ and $Pde9a^{-/-}$, which is consistent with a gene dosage effect of $Pde9a$ on body weight and adiposity (Fig. 7F and L). $Pde9a$ expression in $Pde9a^{+/+}$ mice was compared across dietary treatments, and HFD did not affect its expression in either iBAT or iWAT (Fig. 7F and L and Supplementary Fig. 9F and L). In female iBAT, there were no significant differences in this panel of thermogenic genes between genotypes (Supplementary Fig. 9).

Increased Respiratory Capacity in the BAT of $Pde9a^{-/-}$ Mice

To determine if these changes in thermogenic gene expression altered the function of the iBAT, we performed high-resolution respirometry of iBAT. $Pde9a^{-/-}$ iBAT from both male and female mice demonstrated greater oxygen consumption than $Pde9a^{+/+}$ when the respiratory substrates were added (Fig. 8A and B). This indicates that loss of PDE9 increases the respiratory capacity of the iBAT, even though changes in the expression levels of the components of thermogenesis were not vastly different between genotypes.

DISCUSSION

Analogous to sympathetic nervous system–induced adipocyte browning using the cAMP–cAMP-dependent protein
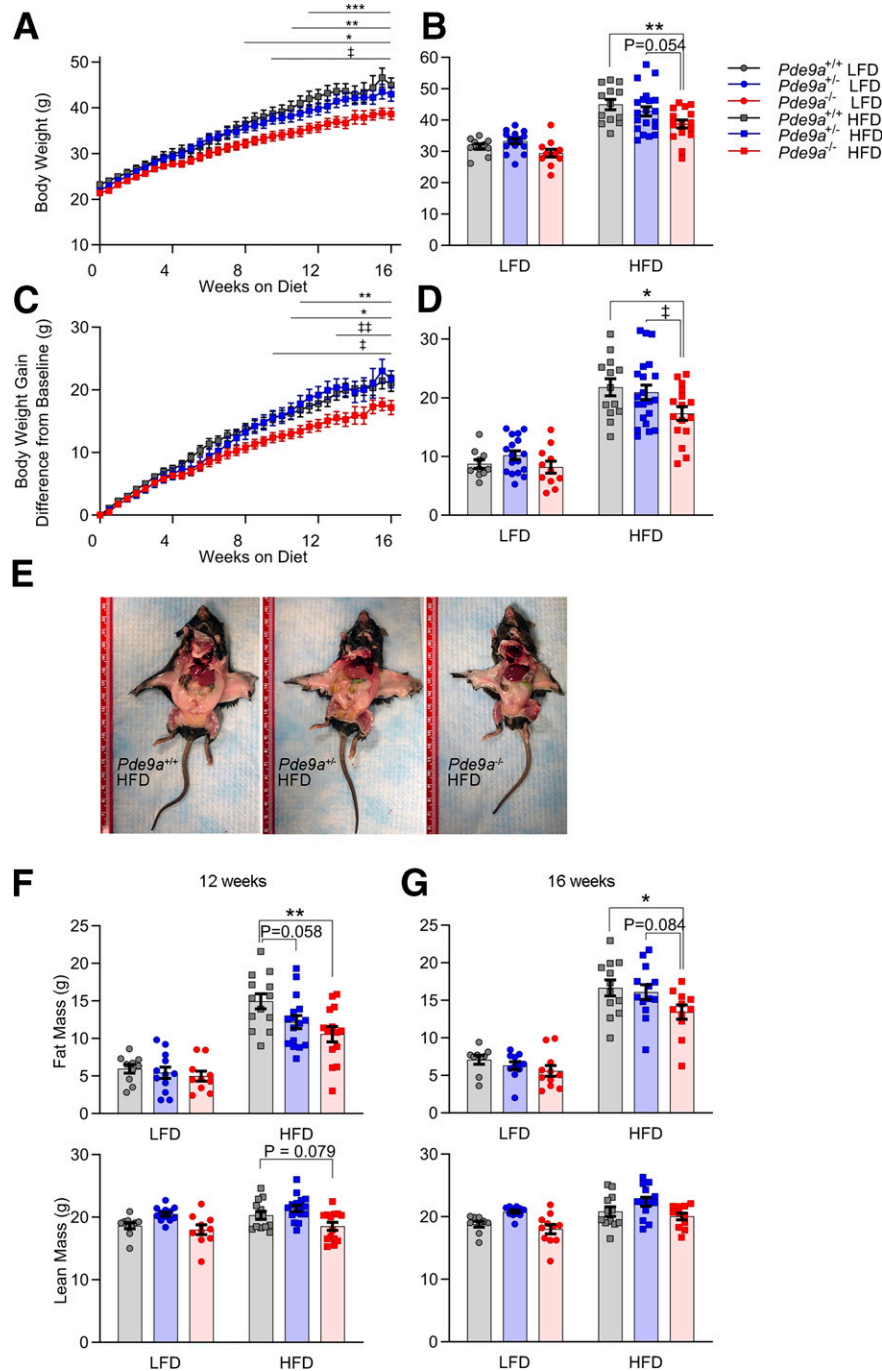
Figure 3—Male $Pde9a^{-/-}$ mice are resistant to diet-induced weight gain and adiposity. *A*: Male $Pde9a^{+/+}$, $Pde9a^{+/-}$, and $Pde9a^{-/-}$ mice were fed an LFD or HFD for 16 weeks beginning at 6 weeks of age. LFD results are in Supplementary Fig. 1. ($P < 0.0001$, genotype × time interaction for HFD; $P = 0.0117$, genotype × time interaction for LFD.) *B*: Terminal body weight ($P = 0.0047$, effect of genotype). *C*: Body weight gain. LFD results are in Supplementary Fig. 1. ($P < 0.0001$, genotype × time interaction for HFD; $P = 0.0118$, genotype × time interaction for LFD.) *D*: Cumulative body weight gain ($P = 0.0387$, effect of genotype). *E*: Representative images of $Pde9a^{+/+}$, $Pde9a^{+/-}$, and $Pde9a^{-/-}$ littermates fed HFD. Body composition at 12 (*F*) and 16 weeks (*G*) of HFD feeding. Data are mean ± SEM. Analyses were performed using two-way ANOVA. For *A* and *C*, two-way ANOVAs were performed with repeated measures. Post hoc analyses were performed using Sidak multiple comparisons test for *Pde9a* genotype only and are indicated on figures with * comparing $Pde9a^{+/+}$ vs. $Pde9a^{-/-}$ and ‡ comparing $Pde9a^{+/-}$ vs. $Pde9a^{-/-}$. * or ‡$P < 0.05$; ** or ‡‡$P < 0.01$. For *A–D*, $N = 10$ $Pde9a^{+/+}$ LFD, 17 $Pde9a^{+/-}$ LFD, 11 $Pde9a^{-/-}$ LFD, 13 $Pde9a^{+/+}$ HFD, 21 $Pde9a^{+/-}$ HFD, and 16 $Pde9a^{-/--/-}$ HFD. For *F* and *G*, $N = 9–10$ $Pde9a^{+/+}$ LFD, 11–12 $Pde9a^{+/-}$ LFD, 10–11 $Pde9a^{-/-}$ LFD, 12–13 $Pde9a^{+/+}$ HFD, 13–16 $Pde9a^{+/-}$ HFD, and 11–14 $Pde9a^{-/-}$ HFD.
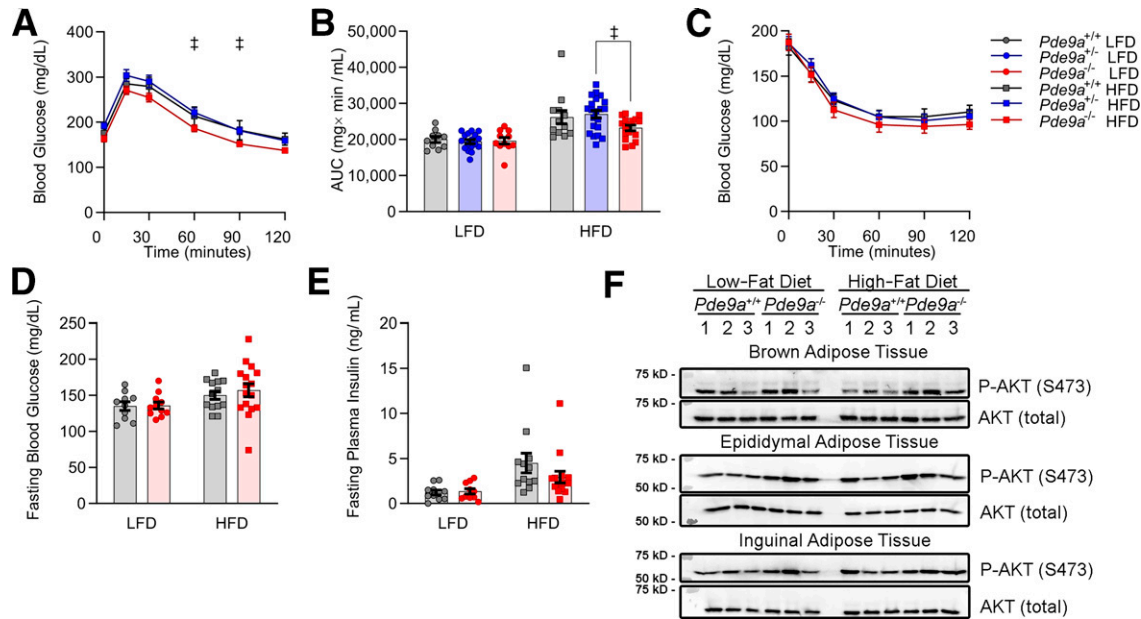
Figure 4—Glucose homeostasis is modestly improved in male $Pde9a^{-/-}$ mice. *A*: IP-GTT in male $Pde9a^{+/+}$, $Pde9a^{+/-}$, and $Pde9a^{-/-}$ mice fed HFD for 15 weeks. *B*: Area under the curve (AUC) of data in *A* and Supplementary Fig. 3. *C*: IP-ITT in male $Pde9a^{+/+}$, $Pde9a^{+/-}$, and $Pde9a^{-/-}$ mice fed HFD for 14 weeks. Five-hour fasting glucose (*D*) and insulin (*E*). *F*: p-AKT at Ser[473] Western blot. Data are mean ± SEM. Analyses were performed using two-way ANOVA. For *A* and *C*, two-way ANOVAs were performed with repeated measures. Post hoc analyses were performed using Sidak multiple comparisons test for $Pde9a$ genotype only and are indicated on figures, with ‡$P < 0.05$ comparing $Pde9a^{+/-}$ vs. $Pde9a^{-/-}$. For *A–E*, N = 10 $Pde9a^{+/+}$ LFD, 17 $Pde9a^{+/-}$ LFD, 10–11 $Pde9a^{-/-}$ LFD, 12–13 $Pde9a^{+/+}$ HFD, 21 $Pde9a^{+/-}$ HFD, and 15–16 $Pde9a^{-/-}$ HFD.

kinase pathway, NP-evoked browning uses cGMP-PKG–mediated signaling (15–17). Stimulation of this pathway has been shown to improve metabolic dysfunction by increasing BAT thermogenesis and browning of WAT (19–25,40–42). Additionally, we have shown that removal of the NP clearance receptor, NPRC, in adipocytes augments cGMP-PKG signaling, leading to increased thermogenic energy expenditure, which consequently reduces obesity and improves glucose handling (20,45). In the present studies, we observed that cold exposure or β₃-AR agonist treatment led to significant decreases in the expression of PDE9, which is highly selective for cGMP (27,28), in brown adipocytes. This observation is like our earlier finding that cold exposure also suppresses the expression of NPRC in AT (20). Therefore, we asked whether genetic deletion of PDE9 would have a similar effect to deletion of NPRC. Interestingly, PDE9 has been suggested to preferentially degrade NP-evoked cGMP (27,37,46). PDE enzymes are already known to play an important role in adipocytes, and nonselective PDE inhibitors have long been known to increase adipocyte lipolysis and thermogenesis (reviewed in Ref. 17). Furthermore, sildenafil, which inhibits the other cGMP-specific PDE expressed in adipocytes, PDE5, has been shown to improve glucose uptake in skeletal muscle and increase energy expenditure (47). While sildenafil did not affect BAT UCP1 expression (47), in a later study, it was

reported to induce browning of iWAT (48). Though PDE9 has been detected in human AT (49), its role in adipose browning and energy balance had not been previously studied.

In this study, we found that inhibition of PDE9 increased PKG signaling and UCP1 expression in adipocytes (Fig. 8C). Global gene deletion of $Pde9a$ resulted in the mice being resistant to HFD-induced obesity due to increased iBAT thermogenic gene expression and an associated increase in energy expenditure. There were no differences in physical activity or food intake ($Pde9a^{-/-}$ mice actually tended to eat slightly more food than $Pde9a^{+/+}$). This reduction in adiposity ameliorated metabolic dysfunction in several ways. Most noticeably, HFD-induced hepatic steatosis and liver damage was greatly reduced in the $Pde9a^{-/-}$ mice. The larger caloric deficit due to energy expenditure in $Pde9a^{-/-}$ mice primarily reduced the hepatic lipid content, with WAT depots somewhat less affected. Thus, in $Pde9a^{-/-}$ mice, lipids were appropriately stored in the adipose instead of elsewhere ectopically. Additionally, glucose handling was modestly improved in the $Pde9a^{-/-}$ compared with $Pde9a^{+/+}$ mice when challenged with HFD. Upon close evaluation of this glucose handling phenotype, we found that these improvements in $Pde9a^{-/-}$ mice were not due to increased glucose uptake or elevated insulin secretion, but rather were due to the reduced adiposity. Nevertheless, as
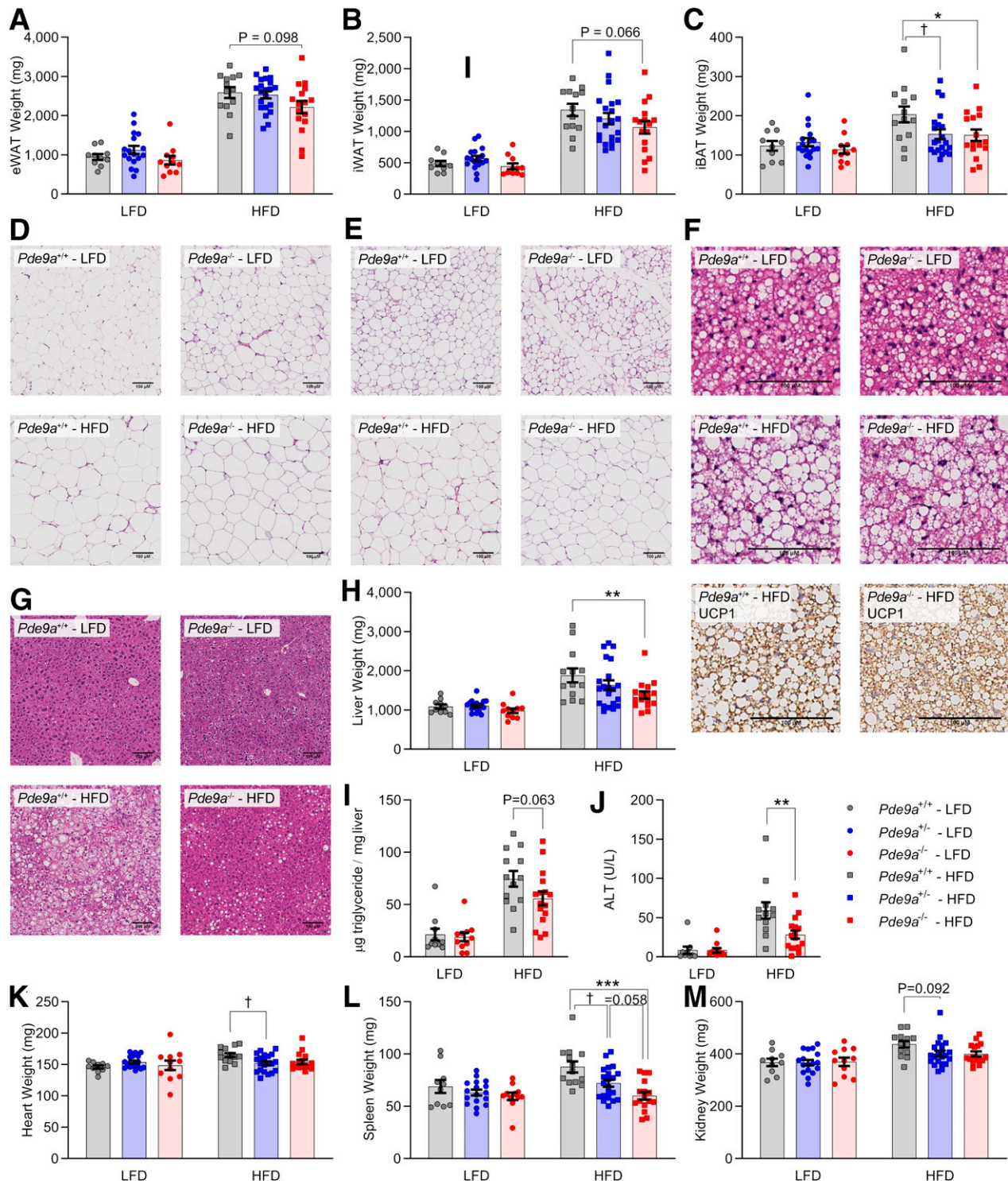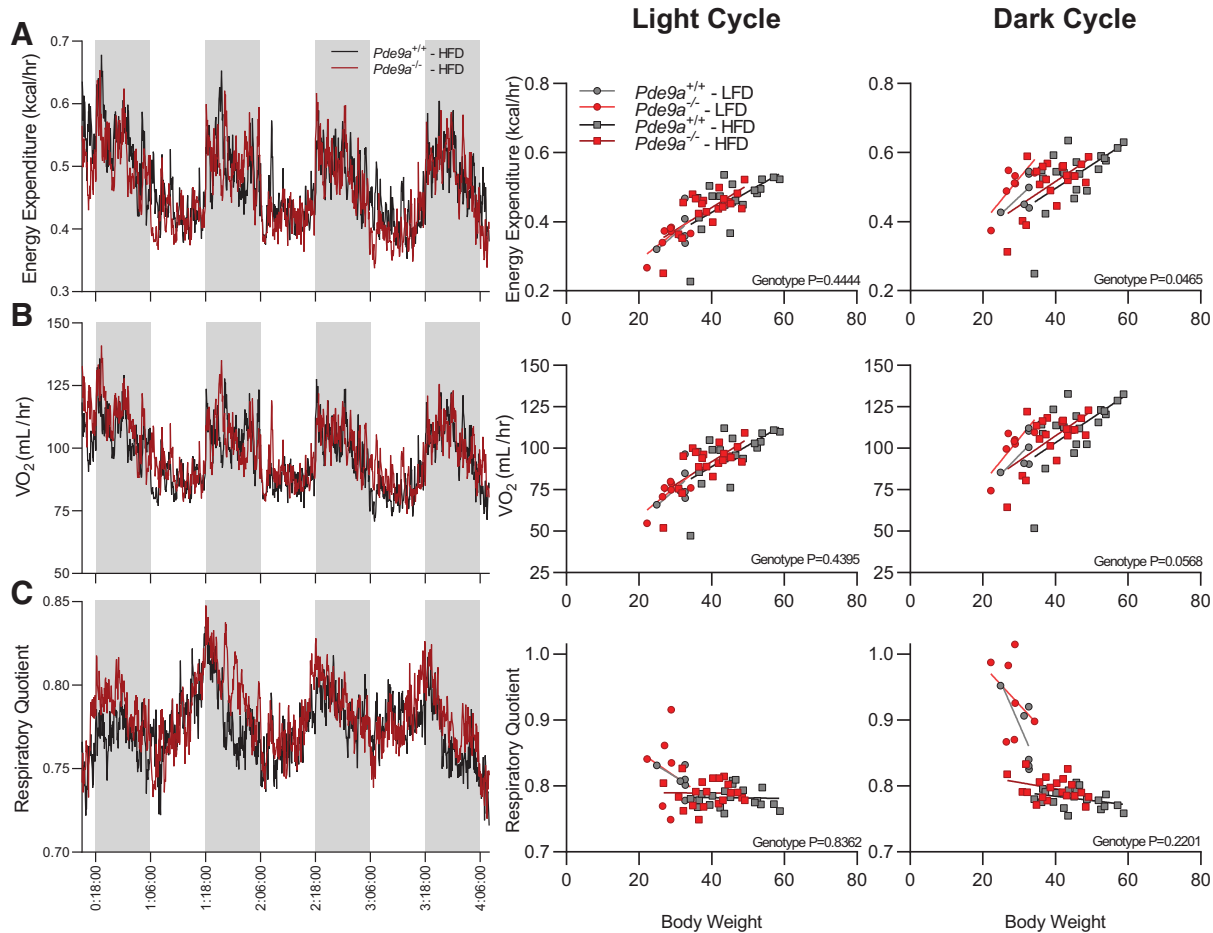
Figure 5—Male *Pde9a*$^{-/-}$ mice are protected from HFD-induced AT expansion and liver damage. *A*: eWAT weights (*P* = 0.049, effect of genotype). *B*: iWAT weights. *C*: iBAT weights. Histology of eWAT (*D*) and iWAT (*E*). *F*: Representative H-E– and UCP1-stained sections of iBAT from HFD-fed mice. *G*: H-E staining of livers. *H*: Liver weights (*P* = 0.039, effect of genotype). *I*: Ratio of hepatic triglyceride to tissue weight. *J*: Plasma ALT (*P* = 0.027, effect of genotype). *K*: Heart weight (*P* = 0.027, effect of genotype × diet interaction). *L*: Spleen weight (*P* = 0.0003, effect of genotype). *M*: Kidney weight. Data are mean ± SEM. Analyses were performed using two-way ANOVA. Post hoc analyses were performed using Sidak multiple comparisons test for *Pde9a* genotype only and are indicated on figures, with * comparing *Pde9a*$^{+/+}$ vs. *Pde9a*$^{-/-}$, † comparing *Pde9a*$^{+/+}$ vs. *Pde9a*$^{+/-}$, and ‡ comparing *Pde9a*$^{+/-}$ vs. *Pde9a*$^{-/-}$. * or †*P* < 0.05; **P* < 0.01; ***P* < 0.001. *N* = 10 *Pde9a*$^{+/+}$ LFD, 17 *Pde9a*$^{+/-}$ LFD, 11 *Pde9a*$^{-/-}$ LFD, 13 *Pde9a*$^{+/+}$ HFD, 21 *Pde9a*$^{+/-}$ HFD, and 16 *Pde9a*$^{-/-}$ HFD. Images are a representative sample from three mice from each group.

Figure 6—*Pde9a*^{−/−} mice have increased energy expenditure. *A*: Energy expenditure increase in *Pde9a*^{−/−} mice in dark cycle (gray; *P* = 0.047, effect of genotype) and light cycle (white; *P* = 0.444, effect of genotype). *B*: Oxygen consumption in *Pde9a*^{−/−} in dark cycle (*P* = 0.057, effect of genotype) and light cycle (*P* = 0.440, effect of genotype). *C*: Respiratory quotient in *Pde9a*^{−/−} mice in dark cycle (*P* = 0.220, effect of genotype) and light cycle (*P* = 0.836, effect of genotype). Values in the figure are the mean from the Promethion System plotted against time (day:hour:minute). Statistics are calculated using the combined data from Promethion and CLAMS using multiple linear regression. See description in RESEARCH DESIGN AND METHODS. *N* = 6 *Pde9a*^{+/+} LFD, 7 *Pde9a*^{−/−} LFD, 20 *Pde9a*^{+/+} HFD, and 20 *Pde9a*^{−/−} HFD.

obesity and increased adiposity are closely associated with impaired insulin sensitivity and poorer glucose handling, PDE9 inhibition has potential as an anti–type 2 diabetes therapeutic. While our findings seem most consistent with a major role for PDE9 in AT, only an adipocyte-specific deletion of *Pde9a* will unequivocally establish its role in this cell type. In contrast, since small-molecule PDE9 inhibitors that are under development and in clinical trials will affect the enzyme wherever it is expressed, the whole-body *Pde9a*^{−/−} mouse serves as preclinical evidence that these inhibitors could have beneficial consequences for metabolic disease.

An unexpected finding of these studies was that *Pde9a*^{+/−} mice displayed an intermediate phenotype. This would suggest a gene dosage effect of *Pde9a*, and thus, even partial inhibition of PDE9 may be able to augment

energy expenditure and improve metabolic disease. Furthermore, this supports the robustness of PDE9 inhibition, as even partial removal of *Pde9a* results in a noticeable improvement in susceptibility to HFD.

PDE9 inhibitors have potential to be useful therapeutics for reducing weight gain and thereby ameliorating associated comorbidities, such as type 2 diabetes. Most importantly, current studies indicate they are safe and well tolerated in humans (28–34). Moreover, analogous to what we show in this study with *Pde9a*^{−/−} mice, our collaborators have found that the PF PDE9 inhibitor reduces body weight by increasing energy expenditure and thereby improves glucose handling in a model of cardiometabolic disease (50). Comparable to our findings, the results of Mishra et al. (50) show that PDE9 inhibition is associated with increased respiration and expression of thermogenic
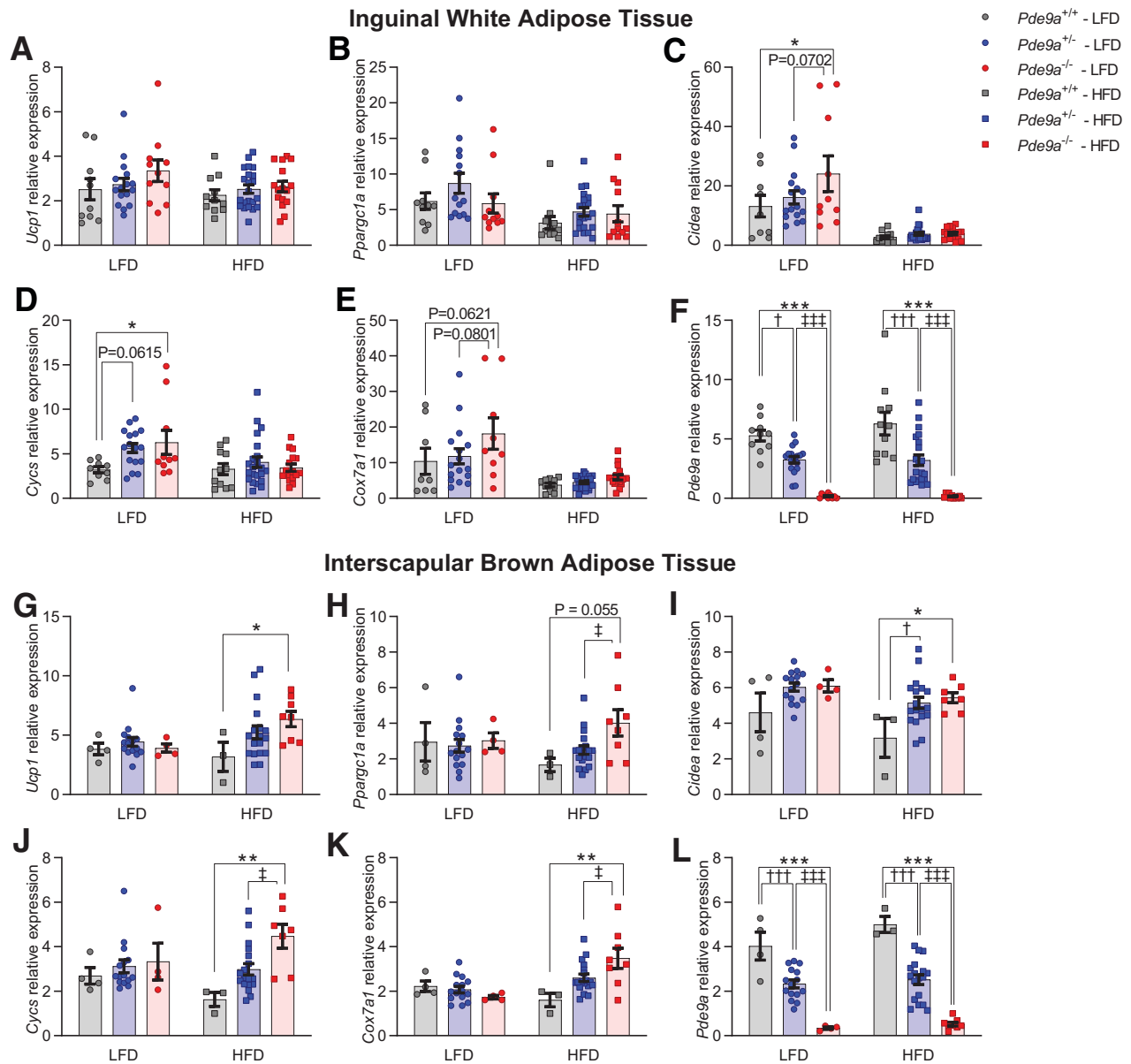
Figure 7—AT of male *Pde9a*$^{-/-}$ mice has increased thermogenic gene expression. The iWAT expression of *Ucp1* (*A*), *Ppargc1a* (*B*), *Cidea* (*C*), *Cycs* (*D*), *Cox7a1* (*E*), and *Pde9a* (*F*) and the iBAT expression of *Ucp1* (*G*), *Ppargc1a* (*H*), *Cidea* (*I*), *Cycs* (*J*), *Cox7a1* (*K*), and *Pde9a* (*L*) by quantitative RT-PCR. Data are mean ± SEM. Analyses were performed using two-way ANOVA. Post hoc analyses were performed using Sidak multiple comparisons test for *Pde9a* genotype only and are indicated on figures, with * comparing *Pde9a*$^{+/+}$ vs. *Pde9a*$^{-/-}$, † comparing *Pde9a*$^{+/+}$ vs. *Pde9a*$^{+/-}$, and ‡ comparing *Pde9a*$^{+/-}$ vs. *Pde9a*$^{-/-}$. *, †, or ‡$P < 0.05$; **$P < 0.01$; ***, †††, and ‡‡‡$P < 0.001$. For iWAT, N = 9–10 *Pde9a*$^{+/+}$ LFD, 14–17 *Pde9a*$^{+/-}$ LFD, 10–11 *Pde9a*$^{-/-}$ LFD, 11 *Pde9a*$^{+/+}$ HFD, 21–22 *Pde9a*$^{+/-}$ HFD, and 12–16 *Pde9a*$^{-/-}$ HFD. For iBAT, N = 4 *Pde9a*$^{+/+}$ LFD, 15 *Pde9a*$^{+/-}$ LFD, 4 *Pde9a*$^{-/-}$ LFD, 3 *Pde9a*$^{+/+}$ HFD, 18 *Pde9a*$^{+/-}$ HFD, and 7–8 *Pde9a*$^{-/-}$ HFD.

genes including *Ucp1* (50). Together, these observations suggest that PDE9 inhibitors can increase thermogenic gene expression in adipocytes via increasing PKG signaling, and these therapeutic implications may be translatable to humans.

Our studies show that loss of *Pde9a* increases iBAT respiratory capacity, modestly increased global energy expenditure, and resulted in an associated decrease in weight gain. At the end of the HFD, this culminated in a large reduction in weight gain and significant metabolic improvements. As most people become obese slowly, a therapeutic approach that blunts weight gain over extended time may be preferable to one that causes rapid reductions in body weight, especially if that approach
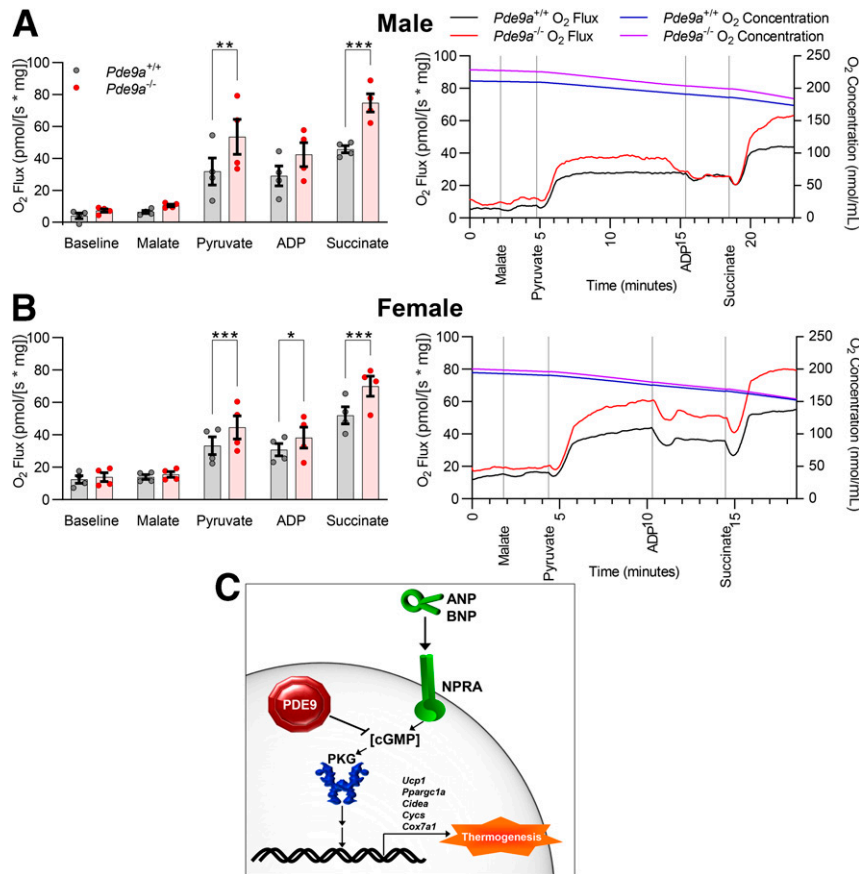
Figure 8—BAT of $Pde9a^{-/-}$ mice has increased respiratory capacity. Average ex vivo oxygen flux in iBAT upon subsequent addition of 0.5 mmol/L malate, 5 mmol/L pyruvate, 5 mmol/L ADP, and 10 mmol/L succinate (left) and representative pairs of high-resolution respirometry traces from male mice (*A*) and female mice (*B*). $N = 4$ for each group. Data are mean ± SEM. Analyses were performed using two-way ANOVA with matching. Post hoc analyses were performed using Sidak multiple comparisons test for $Pde9a$ genotype only and are indicated on figures: *$P < 0.05$; **$P < 0.01$; ***$P < 0.001$. *C*: Summary of adipocyte energy expenditure regulation by PDE9. Loss of PDE9 in $Pde9a^{-/-}$ mice prevents degradation of ANP-evoked cGMP. In adipocytes, this cGMP promotes PKG activation, UCP1 expression, and energy expenditure. The increased energy expenditure protects $Pde9a^{-/-}$ mice from diet-induced weight gain, which mitigates obesity-associated complications, such as poor glucose handling and hepatic triglyceride accumulation.

loses effectiveness over time. Together, these studies suggest that PDE9 inhibition may be a useful approach for augmenting adipose thermogenesis to combat weight gain and improve metabolic health.

References

1. Hales CM, Carroll MD, Fryar CD, Ogden CL. Prevalence of obesity and severe obesity among adults: United States, 2017-2018. NCHS Data Brief 2020;360:1–8

2. Martin-Rodriguez E, Guillen-Grima F, Martí A, Brugos-Larumbe A. Comorbidity associated with obesity in a large population: the APNA study. Obes Res Clin Pract 2015;9:435–447

3. Fothergill E, Guo J, Howard L, et al. Persistent metabolic adaptation 6 years after "The Biggest Loser" competition. Obesity (Silver Spring) 2016;24:1612–1619

4. Laddu D, Dow C, Hingle M, Thomson C, Going S. A review of evidence-based strategies to treat obesity in adults. Nutr Clin Pract 2011;26:512–525

5. Lim R, Beekley A, Johnson DC, Davis KA. Early and late complications of bariatric operation. Trauma Surg Acute Care Open 2018;3:e000219

6. Chen KY, Brychta RJ, Abdul Sater Z, et al. Opportunities and challenges in the therapeutic activation of human energy expenditure and thermogenesis to manage obesity. J Biol Chem 2020;295:1926–1942

7. Arechaga I, Ledesma A, Rial E. The mitochondrial uncoupling protein UCP1: a gated pore. IUBMB Life 2001;52:165–173

8. Wu J, Boström P, Sparks LM, et al. Beige adipocytes are a distinct type of thermogenic fat cell in mouse and human. Cell 2012;150:366–376

9. Min SY, Kady J, Nam M, et al. Human 'brite/beige' adipocytes develop from capillary networks, and their implantation improves metabolic homeostasis in mice. Nat Med 2016;22:312–318

10. van Marken Lichtenbelt WD, Vanhommerig JW, Smulders NM, et al. Cold-activated brown adipose tissue in healthy men. N Engl J Med 2009;360:1500–1508

11. Cypess AM, Lehman S, Williams G, et al. Identification and importance of brown adipose tissue in adult humans. N Engl J Med 2009;360:1509–1517

12. Virtanen KA, Lidell ME, Orava J, et al. Functional brown adipose tissue in healthy adults. N Engl J Med 2009;360:1518–1525

13. Yoneshiro T, Aita S, Matsushita M, et al. Brown adipose tissue, whole-body energy expenditure, and thermogenesis in healthy adult men. Obesity (Silver Spring) 2011;19:13–16

14. Collins S, Bordicchia M. Heart hormones fueling a fire in fat. Adipocyte 2013;2:104–108

15. Pfeifer A, Hoffmann LS. Brown, beige, and white: the new color code of fat and its pharmacological implications. Annu Rev Pharmacol Toxicol 2015;55:207–227

16. Hoffmann LS, Larson CJ, Pfeifer A. cGMP and brown adipose tissue. Handb Exp Pharmacol 2016;233:283–299

17. Ceddia RP, Collins S. A compendium of G-protein-coupled receptors and cyclic nucleotide regulation of adipose tissue metabolism and energy expenditure. Clin Sci (Lond) 2020;134:473–512

18. Shi F, Collins S. Second messenger signaling mechanisms of the brown adipocyte thermogenic program: an integrative perspective. Horm Mol Biol Clin Investig 2017;31:20170062

19. Souza SC, Chau MD, Yang Q, et al. Atrial natriuretic peptide regulates lipid mobilization and oxygen consumption in human adipocytes by activating AMPK. Biochem Biophys Res Commun 2011;410:398–403

20. Bordicchia M, Liu D, Amri EZ, et al. Cardiac natriuretic peptides act via p38 MAPK to induce the brown fat thermogenic program in mouse and human adipocytes. J Clin Invest 2012;122:1022–1036

21. Plante E, Menaouar A, Danalache BA, Broderick TL, Jankowski M, Gutkowska J. Treatment with brain natriuretic peptide prevents the development of cardiac dysfunction in obese diabetic *db/db* mice. Diabetologia 2014;57:1257–1267

22. Glöde A, Naumann J, Gnad T, et al. Divergent effects of a designer natriuretic peptide CD-NP in the regulation of adipose tissue and metabolism. Mol Metab 2017;6:276–287

23. Kimura H, Nagoshi T, Yoshii A, et al. The thermogenic actions of natriuretic peptide in brown adipocytes: the direct measurement of the intracellular temperature using a fluorescent thermoprobe. Sci Rep 2017;7:12978

24. Liu D, Ceddia RP, Collins S. Cardiac natriuretic peptides promote adipose 'browning' through mTOR complex-1. Mol Metab 2018;9:192–198

25. Carper D, Coué M, Nascimento EBM, et al. Atrial natriuretic peptide orchestrates a coordinated physiological response to fuel non-shivering thermogenesis. Cell Rep 2020;32:108075

26. Maurice DH, Ke H, Ahmad F, Wang Y, Chung J, Manganiello VC. Advances in targeting cyclic nucleotide phosphodiesterases. Nat Rev Drug Discov 2014;13:290–314

27. Soderling SH, Bayuga SJ, Beavo JA. Identification and characterization of a novel family of cyclic nucleotide phosphodiesterases. J Biol Chem 1998;273:15553–15558

28. Schwam EM, Nicholas T, Chew R, et al. A multicenter, double-blind, placebo-controlled trial of the PDE9A inhibitor, PF-04447943, in Alzheimer's disease. Curr Alzheimer Res 2014;11:413–421

29. Moschetti V, Boland K, Feifel U, Hoch A, Zimdahl-Gelling H, Sand M. First-in-human study assessing safety, tolerability and pharmacokinetics of BI 409306, a selective phosphodiesterase 9A inhibitor, in healthy males. Br J Clin Pharmacol 2016;82:1315–1324

30. Moschetti V, Kim M, Sand M, et al. The safety, tolerability and pharmacokinetics of BI 409306, a novel and potent PDE9 inhibitor: overview of three phase I randomised trials in healthy volunteers. Eur Neuropsychopharmacol 2018;28:643–655

31. Boland K, Moschetti V, Dansirikul C, et al. A phase I, randomized, proof-of-clinical-mechanism study assessing the pharmacokinetics and pharmacodynamics of the oral PDE9A inhibitor BI 409306 in healthy male volunteers. Hum Psychopharmacol 2017;32:e2569

32. Brown D, Nakagome K, Cordes J, et al. Evaluation of the efficacy, safety, and tolerability of BI 409306, a novel phosphodiesterase 9 inhibitor, in cognitive impairment in schizophrenia: a randomized, double-blind, placebo-controlled, phase II trial. Schizophr Bull 2019;45:350–359

33. Charnigo RJ, Beidler D, Rybin D, et al. PF-04447943, a phosphodiesterase 9A inhibitor, in stable sickle cell disease patients: a phase Ib randomized, placebo-controlled study. Clin Transl Sci 2019;12:180–188

34. Frölich L, Wunderlich G, Thamer C, Roehrle M, Garcia M Jr, Dubois B. Evaluation of the efficacy, safety and tolerability of orally administered BI 409306, a novel phosphodiesterase type 9 inhibitor, in two randomised controlled phase II studies in patients with prodromal and mild Alzheimer's disease. Alzheimers Res Ther 2019;11:18

35. Hutfless S, Maruthur NM, Wilson RF, et al. Strategies to prevent weight gain among adults. Rockville, MD, Agency for Healthcare Research and Quality, March 2013. ARHQ publ. no. 13-EHC029-EF. Accessed 4 September 2020. Available from https://www.ncbi.nlm.nih.gov/books/NBK133218/

36. Malhotra R, Østbye T, Riley CM, Finkelstein EA. Young adult weight trajectories through midlife by body mass category. Obesity (Silver Spring) 2013;21:1923–1934

37. Lee DI, Zhu G, Sasaki T, et al. Phosphodiesterase 9A controls nitric-oxide-independent cGMP and hypertrophic heart disease. Nature 2015;519:472–476

38. Liu D, Bordicchia M, Zhang C, et al. Activation of mTORC1 is essential for β-adrenergic stimulation of adipose browning. J Clin Invest 2016;126:1704–1716

39. Rodriguez A-M, Elabd C, Delteil F, et al. Adipocyte differentiation of multipotent cells established from human adipose tissue. Biochem Biophys Res Commun 2004;315:255–263

40. Miyashita K, Itoh H, Tsujimoto H, et al. Natriuretic peptides/cGMP/cGMP-dependent protein kinase cascades promote muscle mitochondrial biogenesis and prevent obesity. Diabetes 2009;58:2880–2892

41. Coué M, Badin PM, Vila IK, et al. Defective natriuretic peptide receptor signaling in skeletal muscle links obesity to type 2 diabetes. Diabetes 2015;64:4033–4045

42. Bae C-R, Hino J, Hosoda H, et al. Adipocyte-specific expression of C-type natriuretic peptide suppresses lipid metabolism and adipocyte hypertrophy in adipose tissues in mice fed high-fat diet. Sci Rep 2018;8:2093

43. Elabd C, Chiellini C, Carmona M, et al. Human multipotent adipose-derived stem cells differentiate into functional brown adipocytes. Stem Cells 2009;27:2753–2760

44. Smolenski A, Bachmann C, Reinhard K, et al. Analysis and regulation of vasodilator-stimulated phosphoprotein serine 239 phosphorylation in vitro and in intact cells using a phosphospecific monoclonal antibody. J Biol Chem 1998;273:20029–20035

45. Wu W, Shi F, Liu D, et al. Enhancing natriuretic peptide signaling in adipose tissue, but not in muscle, protects against diet-induced obesity and insulin resistance. Sci Signal 2017;10:eaam6870

46. Zhang M, Kass DA. Phosphodiesterases and cardiac cGMP: evolving roles and controversies. Trends Pharmacol Sci 2011;32:360–365

47. Ayala JE, Bracy DP, Julien BM, Rottman JN, Fueger PT, Wasserman DH. Chronic treatment with sildenafil improves energy balance and insulin action in high fat-fed conscious mice. Diabetes 2007;56:1025–1033

48. Mitschke MM, Hoffmann LS, Gnad T, et al. Increased cGMP promotes healthy expansion and browning of white adipose tissue. FASEB J 2013; 27:1621–1630

49. Omar B, Banke E, Ekelund M, Frederiksen S, Degerman E. Alterations in cyclic nucleotide phosphodiesterase activities in omental and subcutaneous adipose tissues in human obesity. Nutr Diabetes 2011;1:e13

50. Mishra S, Hahn V, Sadagopan N, et al. PDE9 inhibition activates PPARα to stimulate mitochondrial fat metabolism and reduce cardiometabolic syndrome. J Clin Invest 2021:e148798